

# Debris Disc Constraints on Planetesimal Formation

Alexander V. Krivov,<sup>1\*</sup> Aljoscha Ide,<sup>1</sup> Torsten Löhne,<sup>1</sup> Anders Johansen,<sup>2</sup>  
and Jürgen Blum<sup>3</sup>

<sup>1</sup>*Astrophysikalisches Institut und Universitätssternwarte, Friedrich-Schiller-Universität Jena, Schillergäßchen 2–3, 07745 Jena, Germany*

<sup>2</sup>*Lund Observatory, Department of Astronomy and Theoretical Physics, Lund University, Box 43, SE-221 00 Lund, Sweden*

<sup>3</sup>*Institut für Geophysik und extraterrestrische Physik, Technische Universität Braunschweig, Mendelssohnstr. 3, 38106, Braunschweig, Germany*

Accepted 2017 November 8. Received 2017 November 8; in original form 2017 September 5

## ABSTRACT

Two basic routes for planetesimal formation have been proposed over the last few decades. One is a classical “slow-growth” scenario. Another one is particle concentration models, in which small pebbles are concentrated locally and then collapse gravitationally to form planetesimals. Both types of models make certain predictions for the size spectrum and internal structure of newly-born planetesimals. We use these predictions as input to simulate collisional evolution of debris discs left after the gas dispersal. The debris disc emission as a function of a system’s age computed in these simulations is compared with several Spitzer and Herschel debris disc surveys around A-type stars. We confirm that the observed brightness evolution for the majority of discs can be reproduced by classical models. Further, we find that it is equally consistent with the size distribution of planetesimals predicted by particle concentration models — provided the objects are loosely bound “pebble piles” as these models also predict. Regardless of the assumed planetesimal formation mechanism, explaining the brightest debris discs in the samples uncovers a “disc mass problem.” To reproduce such discs by collisional simulations, a total mass of planetesimals of up to  $\sim 1000$  Earth masses is required, which exceeds the total mass of solids available in the protoplanetary progenitors of debris discs. This may indicate that stirring was delayed in some of the bright discs, that giant impacts occurred recently in some of them, that some systems may be younger than previously thought, or that non-collisional processes contribute significantly to the dust production.

**Key words:** planetary systems – protoplanetary discs – planets and satellites: formation – comets: general – circumstellar matter – infrared: planetary systems

## 1 INTRODUCTION

Debris discs are belts of leftover planetesimals, i.e., comets and asteroids, around stars (Wyatt 2008; Krivov 2010; Matthews et al. 2014). They are commonly observed through the thermal emission of the dust that these small bodies produce in collisions and other destructive processes. To get insights into the properties of directly invisible planetesimals, observed emission is interpreted by collisional modelling of planetesimal belts, supplemented by thermal emission calculations (e.g. Krivov et al. 2008). A number of prominent discs have been modelled individually this way (e.g. Wyatt et al. 1999; Wyatt & Dent 2002; Thébault et al. 2003; Müller et al. 2010; Reidemeister et al. 2011; Löhne et al. 2012; Schüppler et al. 2014, 2015, 2016). Larger samples of

discs have been modelled on a statistical basis (e.g. Wyatt et al. 2007b; Kennedy & Wyatt 2010; Gáspár et al. 2012, 2013; Pawellek et al. 2014; Pawellek & Krivov 2015; Geiler & Krivov 2017). All these models are able to reproduce the available data and the observed statistical trends reasonably well.

These models, however, typically assume all of the solids to initially have a single power-law size distribution  $dN/dm \propto m^{-\alpha}$  with a slope close to  $\alpha \approx 1.8\dots 1.9$ . A power law with such a slope, which we call “the Dohnanyi slope”, is an analytic solution for the steady-state size distribution found for an idealized collisional cascade (Dohnanyi 1969; O’Brien & Greenberg 2003; Wyatt et al. 2011). The results of elaborate numerical simulations with more realistic physics are expected to deviate from this power law only slightly. This explains why taking it as an initial condition for numerical simulations is so popular: it ensures fast convergence towards

\* E-mail: krivov@astro.uni-jena.de (AVK)

the exact distribution. However, the convenient assumption of an initial Dohnanyi-like slope ignores the fact that the initial size distribution of freshly-formed planetesimals is likely to be very different from Dohnanyi's. As time elapses, larger and larger planetesimals get involved in the collisional cascade. Thus taking another initial distribution of them should affect the modelling results (Löhne et al. 2008).

That primordial size distribution remains poorly known, because so is the process by which planetesimals form. Two basic scenarios have been proposed (see, e.g., Johansen et al. 2014, for a recent review). One is a classical scenario of a slow incremental growth, first by fluffy agglomeration (e.g., Wada et al. 2009; Okuzumi et al. 2012; Wada et al. 2013) or mass transfer from small to large aggregates (e.g., Wurm et al. 2005; Windmark et al. 2012) and then by gravity-driven collisional assemblage of larger planetesimals (e.g., Kenyon & Luu 1999; Kenyon & Bromley 2008; Kobayashi et al. 2010, 2016). Another one is the particle concentration models in which small pebbles are concentrated locally in eddies, pressure bumps or vortices of a turbulent disc (e.g. Haghhighipour & Boss 2003; Cuzzi et al. 2008; Johansen et al. 2009; Cuzzi et al. 2010) or by streaming instability (e.g. Johansen et al. 2007, 2015; Simon et al. 2016, 2017) and then collapse gravitationally to form planetesimals. Both types of models make specific predictions for the size distribution of forming planetesimals, suggesting it to be shallower than Dohnanyi's. They also have implications for the internal structure of planetesimals. For instance, the particle concentration models by Johansen et al. (2015) and Simon et al. (2016, 2017) independently propose  $\alpha \approx 1.6$  over the size range from a few kilometers to a few hundred kilometers and predict planetesimals to be low-density, porous bodies.

The goal of this paper is to check what would happen if we took these predictions by the planetesimal formation models and used them as initial conditions for collisional modelling of debris discs. Would the results still be consistent with debris disc observational data? By comparing the models with the data, we will try to further constrain the initial size distribution and internal structure of planetesimals. Our intention in this work is somewhat similar to the study of Kenyon & Bromley (2008) and Kobayashi & Löhne (2014) who investigated the debris disc evolution, assuming classical “slow growth” planetesimal formation models. For the Solar System, work along these lines has been done by Morbidelli et al. (2009) who showed the size distribution in the asteroid belt to be consistent with “asteroids born big”, hence favouring the particle concentration mechanism of asteroid formation. Vitense et al. (2012) came to the same conclusion for the Kuiper belt.

Section 2 presents the collisional model and Section 3 describes the observational datasets on debris discs. Section 4 compares the model predictions to the observational data. Section 5 discusses the results. Section 6 draws our conclusions.

## 2 MODEL

### 2.1 The code

To model the collisional evolution of the discs, we use the collisional code ACE (“Analysis of Collisional Evolution”;

Krivov et al. 2006; Löhne et al. 2008, 2012; Krivov et al. 2013; Löhne et al. 2017). The code assumes a certain central star and a planetesimal disc of certain size, mass, excitation and other properties as input. The code simulates the collisional evolution of the debris disc, predicting the coupled radial and size distributions of solids — from planetesimals to dust — at different time instants. To compare the simulation results to the observational data, the ACE output is then used to calculate thermal emission of dust. Specifically, we compute the thermal emission fluxes at selected far-infrared wavelengths as functions of system's age.

### 2.2 General parameters

Since resolved images of the vast majority of debris discs show them to be relatively narrow rings with a typical distance from the star of  $\sim 100$  AU (e.g. Pawellek et al. 2014), the reference disc model in all ACE runs was a 10 AU wide ring around a distance of 100 AU. As a central star, we chose an A-type star of 2.16 solar masses with a luminosity of 27.7 times the solar luminosity. The above choices are close to the median values of the samples described below. We are aware, of course, that all these parameters for individual discs in those samples vary considerably. However, we decided to fix them to avoid dealing with an unmanageable set of free parameters and to keep our treatment as simple as possible. This was backed up by several tests to see how the debris disc fluxes and their evolution in time would alter if we varied the luminosity and mass of the host stars, as well as the radius and width of the debris rings. The changes were found to be moderate. The largest quantitative changes arise from variation of the disc radius, consistently with previous studies (see, e.g., top right panel of Fig. 11 in Löhne et al. 2008).

We postulated a disc of planetesimals with eccentricities between 0 and 0.1 and inclinations from 0 to 3 degrees. Here too, we argue that variation of the assumed eccentricity and inclination distribution would not alter the results markedly. Indeed, the collision rates are nearly independent of eccentricities. This is because collisional rates are proportional to the ratio collisional velocity / collisional interaction volume. Both quantities are proportional to eccentricity, which then cancels out (see, e.g., Krivov et al. 2006). The same applies to inclinations. What the eccentricities and inclinations do affect is the collisional velocities. As a result, the dust production rate at higher eccentricities is higher early on, and it decays more rapidly at later times. Quantitatively, however, the effect is only moderate. See, for instance, Fig. 11 (bottom right) in Löhne et al. (2008), which shows the evolution for  $e = 0.05, 0.10, 0.15,$  and  $0.20$ , and a discussion therein.

The solids were assumed to consist of an astrosilicate–water ice mixture in a 30%–70% ratio. Since the material composition of extrasolar comets is not known, this choice is arbitrary. We only made it because silicate–ice mixtures worked better than pure silicate or pure ice in SED fitting of several debris discs studied previously (e.g., Reidemeister et al. 2011; Lebreton et al. 2012; Donaldson et al. 2013; Schüppler et al. 2016). Alternatively, we could have used other compositions, such as mixtures of silicates, ices, carbonaceous materials, and vacuum (e.g., Lebreton et al. 2012; Donaldson et al. 2013) or those involving hydrocarbons that were found to be the major constituent of the comet 67/P

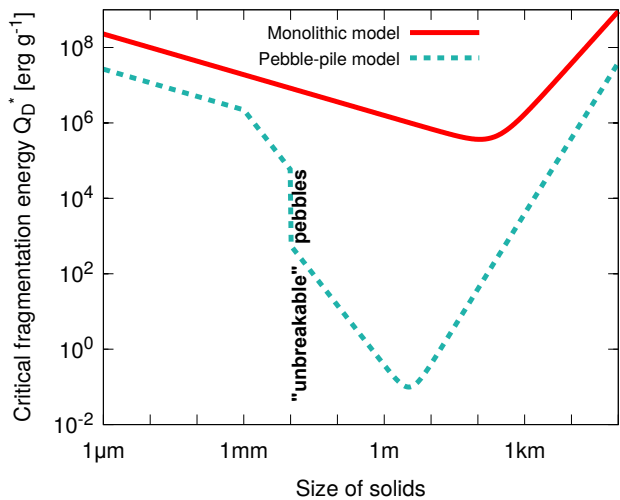


**Figure 1.** Critical fragmentation energy as a function of size (for  $v_{\text{imp}} = 300 \text{ m s}^{-1}$ ). Red solid line: standard “monolithic” model, Eq. (1). Cyan dashed line: pebble-pile model, Eq. (2).

in the Solar System (Fulle et al. 2016). On any account, we do not expect the results to be very sensitive to the material composition chosen. To avoid unnecessary complications, the Poynting-Robertson drag and stellar wind drag were switched off. The solids spanned the size range from  $s_{\text{min}} = 0.2 \mu\text{m}$  to  $s_{\text{max}} = 200 \text{ km}$ .

### 2.3 Critical fragmentation energy

To model the outcomes of collisions between the objects, we also needed to assume a certain critical fragmentation energy, which depends on the material strength, the object size, and the impact velocity  $v_{\text{imp}}$ . We used two prescriptions. One of them is appropriate for “monolithic”, collisionally strong planetesimals in the “slow growth” planetesimal formation models and is taken from Schüppler et al. (2016):

$$Q_{\text{D}}^* = \left[ A_{\text{s}} \left( \frac{s}{1 \text{ m}} \right)^{3b_{\text{s}}} + A_{\text{g}} \left( \frac{s}{1 \text{ km}} \right)^{3b_{\text{g}}} \right] \left( \frac{v_{\text{imp}}}{v_0} \right)^{0.5}, \quad (1)$$

where we set  $v_0 = 3 \text{ km s}^{-1}$  and chose  $b_{\text{s}} = -0.12$ ,  $b_{\text{g}} = 0.46$ , and  $A_{\text{g}} = A_{\text{s}} = 5 \times 10^6 \text{ erg g}^{-1}$ . This prescription is essentially based on the SPH simulations by Benz & Asphaug (1999) for basalt, complemented with the velocity dependence taken from Stewart & Leinhardt (2009). The resulting critical fragmentation energy is plotted in Fig. 1.

In addition to prescription (1), we also tried an alternative model for  $Q_{\text{D}}^*$  that we deem more suitable for planetesimals forming through the particle concentration mechanism. In this scenario, planetesimals are likely piles of cm-sized pebbles (Johansen et al. 2015). Based on recent laboratory experiments on the strength of dust aggregates (Bukhari Syed et al. 2017; Whizin et al. 2017), we can formulate the following prescription for  $Q_{\text{D}}^*$ :

$$Q_{\text{D}}^* = A_{\text{pp}} \left( \frac{s}{1 \text{ mm}} \right)^{3b_{\text{pp}}} \left( \frac{v_{\text{imp}}}{v_0} \right)^{0.5} + \frac{3Gm}{5s}, \quad (2)$$

where

$$A_{\text{pp}} = \begin{cases} 7 \times 10^6 \text{ erg/g} & \text{for } s < 1 \text{ cm,} \\ 7 \times 10^4 \text{ erg/g} & \text{for } s > 1 \text{ cm} \end{cases} \quad (3)$$

and

$$b_{\text{pp}} = \begin{cases} -0.12 & \text{for } s < 1 \text{ mm,} \\ -0.53 & \text{for } s > 1 \text{ mm.} \end{cases} \quad (4)$$

In the last term in Eq. (2),  $G$  is the gravitational constant, and  $m$  is the mass of an object of radius  $s$ . We arrived at Eq. (2) by using the velocity scaling derived by Bukhari Syed et al. (2017), i.e.,  $Q_{\text{D}}^* \propto s^{3b_{\text{pp}}} \propto s^{-1.58}$ , measured for pebble piles that were compacted to rather homogeneous dust aggregates with filling factors of 0.35. To account for the much lower cohesion within uncompacted (i.e., primordial) pebble piles, we scaled the pre-factor  $A_{\text{pp}}$  in Eq. (2) accordingly (see Eq. (3) and Fig. 1). Our scaling is based on the experimental data by Whizin et al. (2017) and Bukhari Syed et al. (2017). Whizin et al. (2017) experimentally investigated the collision behaviour of cm-sized pebble clusters. Extrapolating their data to collisions among equal-sized clusters yields a fragmentation threshold of  $\sim 1 \text{ cm s}^{-1}$ . This is well below the respective value for compacted dust aggregates, which was determined by Bukhari Syed et al. (2017) to be on the order of  $1 \text{ m s}^{-1}$ .

When using the model (2), the size distribution of fragments resulting from the disruption of pebble aggregates was assumed to have a lower cutoff at the pebble size. To describe the disruption of pebbles themselves, we used the fragment size distribution extending down to sub-micron-sized dust.

In Fig. 1, we compare this pebble-pile  $Q_{\text{D}}^*(s)$  model with the monolithic one. The critical fragmentation energy given by Eq. (2) falls off more steeply for  $s > 1 \text{ mm}$  (with  $b_{\text{pp}} = -0.53$ ) and features an additional drop by two orders of magnitude at the boundary between pebbles ( $s \lesssim 1 \text{ cm}$ ) and pebble piles ( $s \gtrsim 1 \text{ cm}$ ). Altogether, it is seen that the pebble-pile model predicts much weaker planetesimals with radii between the pebble size and about one kilometer. The change in the material strength at the dust sizes is less than by order of magnitude. This, rather moderate, change reflects a difference between the simulation results by Benz & Asphaug (1999) and laboratory measurements by Whizin et al. (2017), who also assumed different materials and compositions. Finally, in the gravity regime, the strength of pebble-pile planetesimals differs from that of monolithic objects, too (Stewart & Leinhardt 2009; Leinhardt & Stewart 2012). This is because the propagation of shock waves triggered by the impact through the target and energy dissipation within the target in these two cases are different. As a result, the critical fragmentation energy of pebble-pile objects is dominated by pure gravitational binding energy (the last term in Eq. (2)). This leads to  $Q_{\text{D}}^* \propto s^2$  for  $s \gtrsim 10 \text{ m}$ .

### 2.4 Initial size distribution

Given the goals of this study, the initial size distribution was modelled with two power laws, a steeper one below a certain size and a shallower one above it (Fig. 2). The first one was assumed to have a Dohnanyi-like slope  $\alpha = (11 + 3b_{\text{s}})/(6 + 3b_{\text{s}}) = 1.88$  (O’Brien & Greenberg 2003). Here,  $b_{\text{s}}$  is the slope of  $Q_{\text{D}}^*(s)$  in the strength regime (see Eq. 1). The second

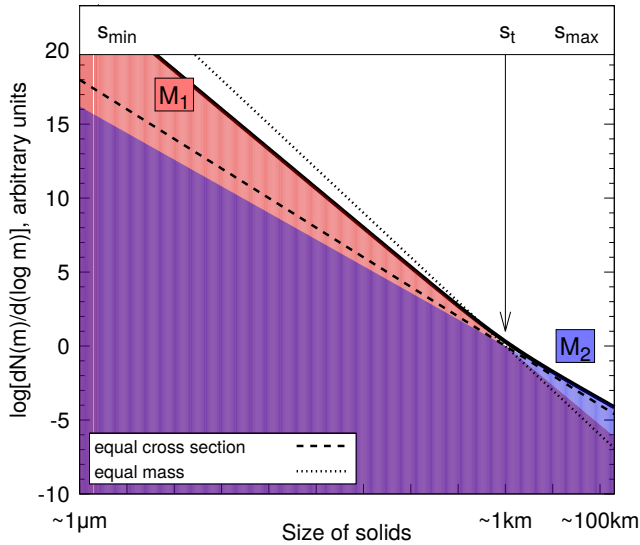


**Figure 2.** Initial size distribution of planetesimals assumed in the collisional simulations (black solid line). It involves two slopes: a steeper one for small solids of sizes  $s_{\min}$  to  $s_t$  (population 1, red-filled area) and a flatter one appropriate for large objects with sizes from  $s_t$  to  $s_{\max}$  (population 2, blue-filled area). Dashed line indicates a slope ( $\alpha = 5/3$ ), for which the *cross section* of solids would be the same in all logarithmic size (or mass) bins. Similarly, dotted line marks the slope ( $\alpha = 2$ ), for which all logarithmic size bins would carry equal *mass* of material.

power law was a proxy for the primordial size distribution of large planetesimals right after the gas dispersal. Accordingly, we used  $\alpha = 1.6$  as expected in both planetesimal formation scenarios considered here.

Since the ACE code does not allow for using broken power-laws, the technical implementation was slightly different. We took two initial populations of solids at the same spatial location — one with a steeper and another one with a shallower power law, as described above. Of course, both populations were let to interact with each other collisionally.

This two-population setup has two free parameters: the total initial disc mass,  $M_1 + M_2$ , and the mass ratio of the two populations,  $M_1/M_2$ . Fixing a ratio  $M_1/M_2$  is equivalent to selecting a certain “turnover” size  $s_t$ , at which the two populations contain equal numbers of planetesimals (Fig. 3). Varying both parameters, and selecting either Eq. (1) or Eq. (2) for  $Q_D^*(s)$ , we try to reproduce the observed level of disc brightness in the far-infrared and its decay towards older ages.

It is easy to see that different combinations of  $M_1/M_2$  (or  $s_t$ ) together with different  $Q_D^*(s)$  prescriptions allow us to test both “slow-growth” and “particle concentration” models of planetesimal formation:

(1) In the slow-growth scenario, growth of larger bodies in a protoplanetary disc is always accompanied with fragmentation at smaller sizes. As the gas density goes down, the collisional cascade induced by growing embedded stirrers produces ever smaller solids, so that by the time when the disc gets gas-free all solids down to dust sizes are generated. As a result, we expect a Dohnanyi-like slope at sizes below about a kilometer and a shallower slope for larger bod-

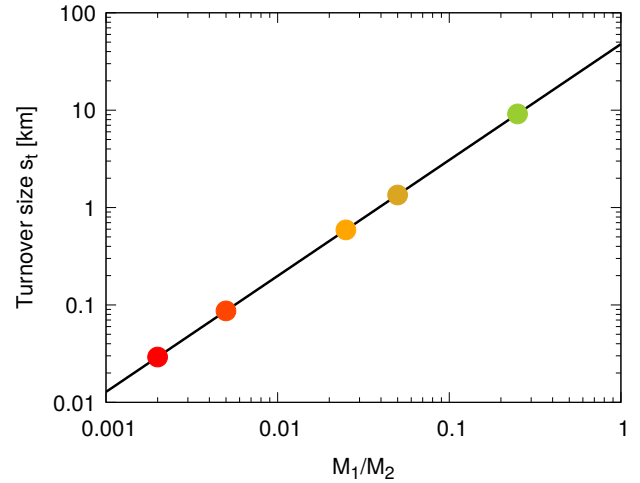


**Figure 3.** Planetesimals’ turnover size as a function of  $M_1/M_2$ . Bold dots mark mass ratios  $M_1/M_2 = 1/4, 1/20, 1/40, 1/200,$  and  $1/500$  assumed to produce the “evolutionary tracks” in Fig. 5. Each mass ratio is associated with a certain colour; the same colour coding is consistently used throughout the paper.

ies that have grown in the disc. Those bodies are expected to be relatively compact (“monolithic”). This means that our two-population setup with  $s_t$  in the kilometer range, together with Eq. (1) for  $Q_D^*(s)$ , is a proxy for the “slow growth” scenario.

(2) In the particle concentration scenario, the expectation is different. Pebbles are efficiently consumed to quickly build large planetesimals with sizes above a few kilometers with a shallower size distribution. These will be loosely bound, having a pebble-pile structure. Fragmentation only plays a minor role, and by the moment of gas dispersal no Dohnanyi-like tail of subkilometer-sized solids is predicted. In terms of our two-population setup, population 1 will be nearly absent (very small  $M_1/M_2$ , or  $s_t \ll 1$  km). Thus taking a small  $s_t$  together with Eq. (2) for  $Q_D^*(s)$  serves as a proxy for the “particle concentration” scenario.

(3) With the same setup, we can also test the traditional debris disc models that do not utilise predictions of planetesimal formation models at all, just using a Dohnanyi-like initial size distribution across the entire size range. To this end, it is sufficient to discard population 2 (by setting  $M_1/M_2$  to infinity, or  $s_t$  to  $s_{\max}$ ) and use Eq. (1) for  $Q_D^*(s)$ .

## 2.5 Typical simulation results

We have performed several ACE simulations with fiducial discs. In all these runs, the disc mass  $M_1 + M_2$  was arbitrarily set to the same value of  $100M_\oplus$ , while the mass ratio between the two populations  $M_1/M_2$  was varied from infinity (no population 2, “traditional” choice) to  $1/500$  (almost all the mass in population 2). All of the runs were done with monolithic planetesimals, except for one where we assumed pebble piles.

Figure 4 plots the size distribution of solids for some of the ACE runs. Both the initial distribution and an evolved one after 100 Myr of collisional grinding are depicted. The



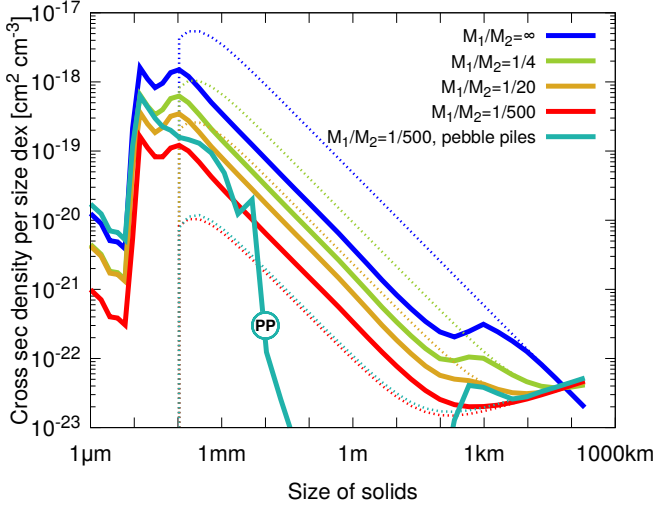


**Figure 4.** Initial (thin dotted) and evolved (after 100 Myr; thick solid) size distributions of material in several fiducial debris discs, produced by ACE simulations. Different runs assumed the same total disc mass of  $100M_{\oplus}$ , but different mass ratios between the two populations. One of the curves (cyan, labelled “PP”) is the  $M_1/M_2 = 1/500$  model assuming the alternative  $Q_D^*$  model appropriate for pebble piles.

initial size distribution is a sum of the two distributions sketched in Fig. 2. Note that Fig. 4 plots the cross section surface density per unit size decade, whereas Fig. 2 depicts the number of solids per unit decade in mass. This explains a somewhat different appearance of the two figures. For instance, horizontal lines in Figure 4 (i.e., lines with a zero slope) would correspond to a slope  $\alpha = 5/3$  in Fig. 2.

We start with discussing the initial distributions. We see that low  $M_1/M_2$  (or  $s_t$ ) cases have an initial deficit of small grains (which are the ones that are seen by mid-IR surveys). Such discs need time to become bright. This is the time it takes to erode enough bigger objects in the initial size distribution in order to refill the initially missing dust population. Such a refill occurs because collisional cascade produces fragments following an  $\alpha \approx 1.9$  size distribution that is steeper (and thus more small-dust “friendly”) than the initial  $\alpha = 1.6$  one.

Further, Fig. 4 illustrates how evolved distributions of solids look like. Common to all of the curves is a sharp cutoff at several micrometers, which is a classical radiation pressure blowout limit (Burns et al. 1979). The grains on the left of it are nearly absent, as these are placed by radiation pressure in hyperbolic orbits and leave the disc on dynamical timescales. Above the blowout limit, the size distributions develop some ripples. This “waviness” is also well known (Campo Bagatin et al. 1994; Krivov et al. 2006; Thébault & Augereau 2007) and is a natural consequence of a sharp blowout cutoff and of a mass loss rate being independent of size in logarithmic bins (Wyatt et al. 2011). Going to larger sizes, a local minimum appears at 100s of meters for “monolithic” curves, which simply mirrors the minimum of the critical fragmentation energy (see. Eq. 1).

This “mirroring” of  $Q_D^*$  by the size distribution is best illustrated with the alternative  $Q_D^*$  model. Figure 4 shows

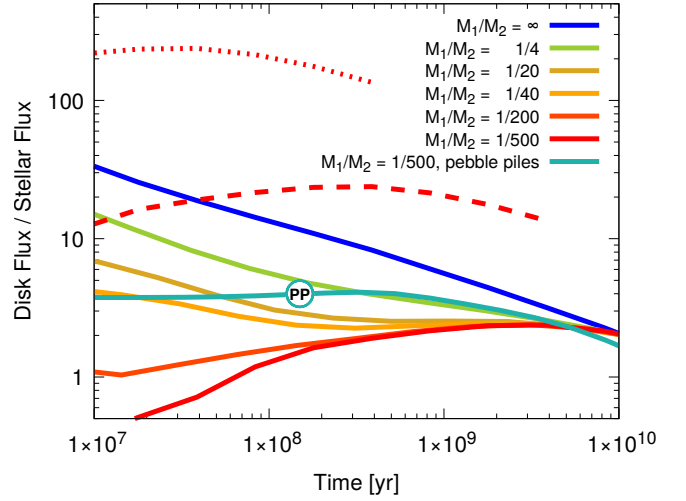


**Figure 5.** Time evolution of a  $70\mu\text{m}$  flux from several fiducial debris discs, resulting from ACE simulations. The colour coding is the same as in Fig. 4. For the  $M_1/M_2 = 1/500$  model, the dashed and dotted lines show the flux evolution for discs with  $1000M_{\oplus}$  and  $10,000M_{\oplus}$  respectively. This illustrates the scaling described in the text, see Eq. (5).

how a significant difference between the two models for the critical fragmentation energy (1) and (2) causes a dramatic difference in the evolved size distribution. This result is not surprising, as even the moderate changes in the critical fragmentation energy have been shown to alter the size distribution markedly (e.g. Thébault & Augereau 2007; Gáspár et al. 2012). However, it is for the first time that such an extreme model for  $Q_D^*$  is being studied. The cyan curve, produced with the alternative  $Q_D^*$  model, develops a pronounced minimum at sizes where  $Q_D^*$  itself has a deep minimum. The means that the disc contains a low number of pebble piles that are small enough not to be kept together by gravity.

For each of the runs, we have also computed a time evolution of the dust emission flux at  $70\mu\text{m}$ . Figure 5 shows the results. For the standard fragmentation energy model, the disc brightness decreases from higher to smaller  $M_1/M_2$  ratios. At the same time, the flux decay slows down. In fact, for a very pronounced population 2 the disc brightness first goes up until the decay sets in (see the  $M_1/M_2 = 1/200$  and  $M_1/M_2 = 1/500$  curves). All this is because discs with a heavy population 2 contain nearly all their mass in the large planetesimals, and there is initially not enough dust to emit. That dust has first to be produced collisionally, which takes time.

This is different in the run that assumed an alternative  $Q_D^*$  model. In this case, planetesimals are fragile pebble piles that are collisionally destroyed very quickly. This is because the pebble piles can be disrupted by much smaller projectiles than the monolithic planetesimals of the same size, and the collisional rates with smaller projectiles are much higher. A debris disc consisting of such fragile planetesimals produces enough dust promptly, even if population 1 is absent. This is demonstrated by a cyan curve in Figure 5 that presents the  $M_1/M_2 = 1/500$  model for the alternative  $Q_D^*$  prescription.

While Fig. 5 presents the luminosity evolution of discs

of the same total mass, it is also important to understand how a change in the total mass would alter the evolution. To interpret the time evolution of discs with different initial masses, there is a useful analytic scaling (Löhne et al. 2008; Krivov et al. 2008). Consider a disc with initial mass  $M_0$  at a distance  $r$  from the star with age  $t$ . Denote by  $F(M_0, r, t)$  any quantity directly proportional to the amount of disc material in any size regime, from dust grains to planetesimals. For instance,  $F$  may stand for the total disc mass, the mass of dust, its total cross section, or dust emission flux at any wavelength. The scaling rule reads:

$$F(xM_0, r, t) = xF(M_0, r, xt), \quad (5)$$

valid for any factor  $x > 0$ . Equation (5) holds for every disc of particles, as long as these are produced, modified and lost in binary collisions and not in any other physical processes. Figure 5 illustrates, for one of the models, how the scaling works. When the initial mass of the disc increases, the flux evolution curve moves leftward and upward without changing its shape.

### 3 OBSERVATIONAL DATA

To compare the collisional models with data, we chose to consider A-type stars. There are more detections around A-type stars, providing better statistics. Besides, the discs around A-type stars are known to exhibit a more rapid decay of the dust luminosity towards older systems than discs of solar-type stars (Wyatt 2008). We selected three datasets:

- a Spitzer/MIPS 70  $\mu\text{m}$  sample of A-type stars from Su et al. (2006) that contains 69 excess stars with  $S/N > 3$  (out of 137 in total) with ages between 5 and 850 Myr;
- a collection of Spitzer/MIPS 70  $\mu\text{m}$  data for different-type stars of Chen et al. (2014). From this, we extracted A-stars only (145 detections out of 149 observed A-type, 3 to 1360 Myr-old stars);
- a Herschel/PACS 100  $\mu\text{m}$  sample for A-type stars from Thureau et al. (2014). This includes 18 sources with a flux excess significance  $> 3$  among 83 stars with ages from 12 to 800 Myr.

These three samples are visualized in Fig. 6. It plots the excess ratios (i.e., dust fluxes divided by the stellar photospheric flux) versus stellar age. Before we proceed with a comparison between these data and collisional models, we make several remarks about the data themselves.

First, Chen et al. (2014) and Thureau et al. (2014) also performed the SED fitting of the excess stars. They tried both single- and two-temperature fits and concluded that many of the discs are likely to have a two-component structure, including an additional warm component closer to the star. Since we discuss the cold Kuiper-belt analogs in this paper, it would be reasonable to subtract the contribution of the warm component from the total disc flux. We now estimate this contribution. Denote the temperatures of the warm and cold components by  $T_w$  and  $T_c$ , and their fractional luminosities by  $f_w$  and  $f_c$ , respectively. Next, let  $R_w(\lambda)$  and  $R_c(\lambda)$  be the excess ratios for the two components. Assuming both components to emit as black bodies,

it is easy to derive

$$\frac{R_w(\lambda)}{R_c(\lambda)} = \left(\frac{f_w}{f_c}\right) \left(\frac{T_w}{T_c}\right)^{-4} \left[\frac{B_\nu(T_w, \lambda)}{B_\nu(T_c, \lambda)}\right], \quad (6)$$

where

$$B_\nu(T, \lambda) = \frac{2hc}{\lambda^3} \left[\exp\left(\frac{hc}{\lambda kT}\right) - 1\right]^{-1}$$

is the Planck intensity in the frequency scale as a function of temperature and wavelength, with  $h$  being Planck constant,  $c$  the speed of light, and  $k$  the Boltzmann constant. For the Chen et al. (2014) sample, the average values are  $T_w = 300$  K,  $T_c = 100$  K,  $f_w = 6 \times 10^{-5}$ , and  $f_c = 1 \times 10^{-4}$ . Equation (6) gives  $R_w/R_c$  as small 2.9% at 70  $\mu\text{m}$  and 2.2% at 100  $\mu\text{m}$ , showing that the contribution of the inner component to the observed flux at 70  $\mu\text{m}$  and 100  $\mu\text{m}$  is almost negligible. We decided against making this correction for the sake of simplicity.

Second, there are some caveats about the datasets that are related to the brightest discs with excess ratios of  $\gtrsim 100$ , which are the most numerous in the Chen et al. (2014) sample. These discs can be loosely classified into two groups, the old ( $> 100$  Myr) and the young ones ( $< 100$  Myr), and we now discuss these two groups in turn. The brightest discs around stars listed as having ages 100 Myr and more in their sample, most of which do not belong to clusters, may in fact be considerably younger according to independent age estimates reported in the literature. For example, HD 54341 has a reported age of 364 Myr in Chen et al. (2014), while an age estimation based on isochrones suggest a much younger age of 10 Myr (Rhee et al. 2007). The same applies to several other bright discs reported by Chen et al. (2014) to be old — they all may be much younger. These include HD 12467 (200 Myr instead of 776 Myr, see Rhee et al. 2007), HD 24966 (100 Myr instead of 364 Myr, see Moór et al. 2006), and HD 120534 ( $< 320$  Myr instead of 400 Myr, see Moór et al. 2006). This would push the bright but old discs to much younger ages, where high dust luminosities are readily expected. For bright discs around stars younger than 100 Myr, it is likely that the “collisional” ages of our numerical model do not necessarily correspond to the system ages. Some discs could have started the collisional cascade later in their lifetimes due to delayed stirring; we will discuss this in Section 5.3. Finally, in many of the youngest, bright discs that fill the left upper corner in the middle panel of Fig. 6, gas has been detected (e.g., Moór et al. 2011; Kral et al. 2017). There is an uncertainty of whether those are true debris discs or are still in the protoplanetary or transitional phase. Our model would not be applicable to such systems.

Another star with a bright disc in the Pleiades (age of  $\approx 100$  Myr) in the Chen et al. (2014) sample, HD 23642, is an eclipsing binary with a period of about 2.5 days (see Southworth et al. 2005, where also the stellar parameters are given). Fitting a model photosphere of a single star to the binary star will underestimate the IR luminosity of the binary, if the smaller companion is colder than the primary one. This happens because the bright and hot star dominates the flux at short wavelengths where the fitting takes place, but the influence of the companion grows at the longer wavelengths, meaning the flux ratio of secondary to primary star,  $F_B(\lambda)/F_A(\lambda)$ , is larger in far-IR. For HD 23642, this flux ratio is about 30% higher at 70  $\mu\text{m}$  than at 1  $\mu\text{m}$ . Tak-

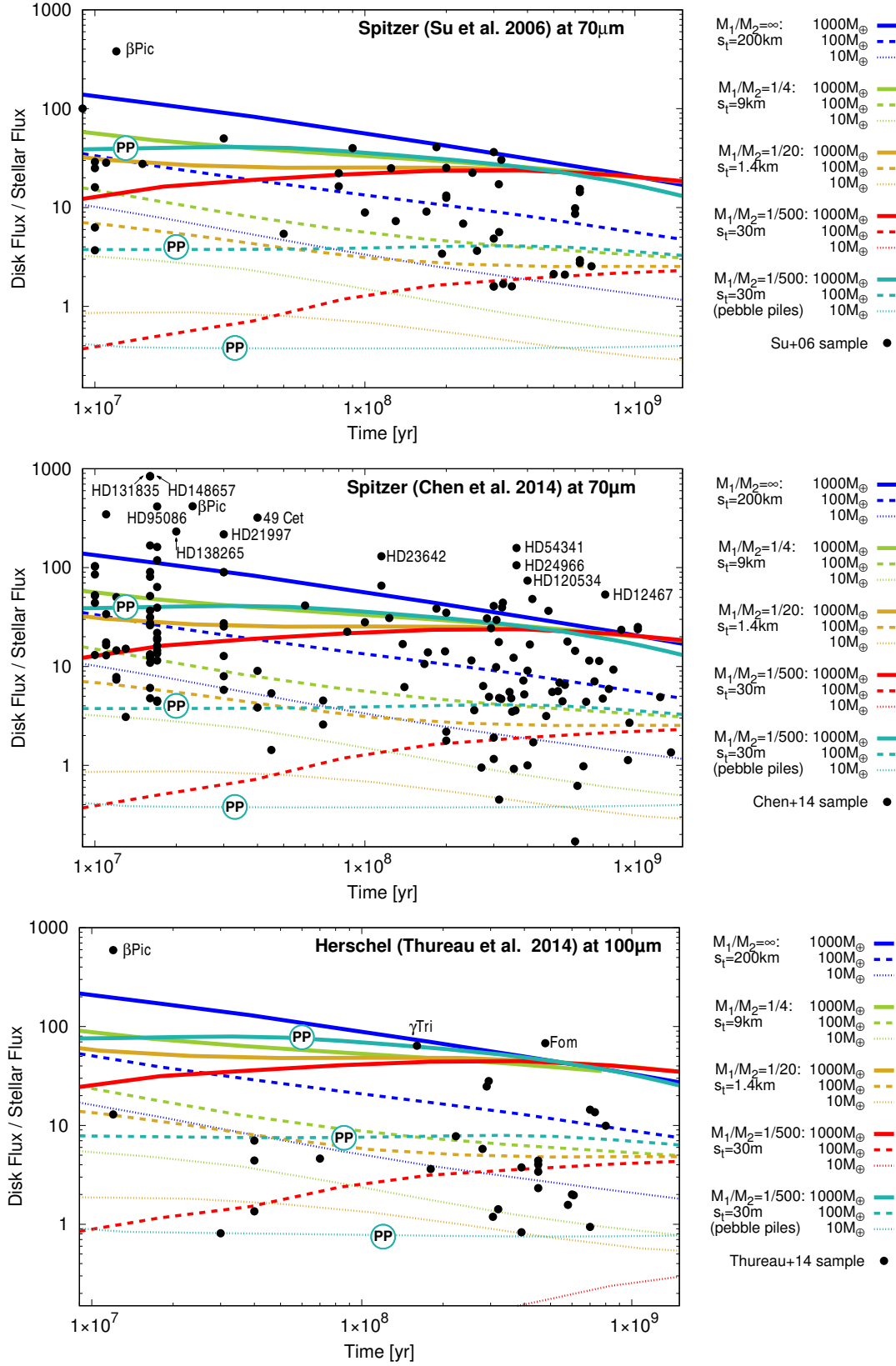


**Figure 6.** Samples from Su et al. (2006) (top), Chen et al. (2014) (middle), and Thureau et al. (2014) (bottom) and the ACE models. Symbols are flux ratios inferred from observations through the SED fitting, as published in the original papers. A few prominent discs are labelled. Lines are ACE models (different colours and linestyles for different  $M_1/M_2$ , and different line thicknesses for different  $M_1 + M_2$ ). For each  $M_1/M_2$ , three curves for  $M_1 + M_2$  of 10, 100, and 1000 Earth masses are shown. As in previous figures, the cyan curves labelled “PP” correspond to  $M_1/M_2 = 1/500$  and the alternative  $Q_D^*$ .

ing this effect into account reduces the flux ratio for the disc of HD 23642 from 130 as reported by [Chen et al. \(2014\)](#) to  $130 \times (1 + F_B(1 \mu\text{m})/F_A(1 \mu\text{m})) / (1 + F_B(70 \mu\text{m})/F_A(70 \mu\text{m})) \approx 125$ . Although the correction is moderate, it may affect a number of discs, since some of their host stars may have as yet unknown colder companions. In addition, close binarity may directly influence the discs by perturbing and stirring them.

#### 4 MODEL VS DATA

Figure 6 compares the [Su et al. \(2006\)](#), [Chen et al. \(2014\)](#), and [Thureau et al. \(2014\)](#) data with our collisional model for different choices of  $M_1 + M_2$  and  $M_1/M_2$ . All of the simulations but one assumed the standard  $Q_D^*$  model (Eq. 1). One simulation was run with the alternative  $Q_D^*$  assuming pebble piles (Eq. 2). In each case, three curves are presented, corresponding to the  $M_1 + M_2 = 10, 100,$  and  $1000M_\oplus$ .

##### 4.1 Discs of “monolithic” planetesimals

We start with a discussion of the runs done with a standard  $Q_D^*$  (i.e., “monolithic” planetesimals). We compare the simulations with the data in the order of decreasing  $M_1/M_2$  (or increasing  $M_2$ , or decreasing  $s_t$ ). Purely “traditional” models, i.e., those without population 2, reproduce both the mean emission level and its long-term decay with the stellar age at disc masses of 10–100  $M_\oplus$ . This is consistent with [Wyatt et al. \(2007b\)](#) who derive a mean disc mass of 10  $M_\oplus$  (assuming  $s_{\text{max}}$  of 30 km) in their population model designed to reproduce the sample of discs around A-type stars from [Rieke et al. \(2005\)](#). Adding the “non-traditional” population 2 with  $s_t$  at several kilometers, we are still able to reproduce the data, as expected (see Fig. 5 and a discussion of it). However, the disc masses  $M_1 + M_2$  needed to reach the observed emission level increase. Between almost a hundred and a few hundred of Earth masses are now needed to match the discs of average brightness.

Decreasing  $s_t$  to about one kilometer leads to growing discrepancies between the data and models. The decay slows down. For  $s_t \sim 1$  km (see the  $M_1/M_2 = 1/20$ , or  $s_t = 1.4$  km curves), the flux evolution gets nearly flat. For yet smaller  $s_t$ , the disc brightness evolution is no longer monotonic. Instead, it first increases for at least 100 Myr and only then starts to decrease (see  $M_1/M_2 = 1/500$  or  $s_t = 30$  m curves), which is inconsistent with the data. Even though the scatter of points at any given age is large, it is obvious that the models that only include population 2 do not provide any acceptable fits to the observed trend. This tells us that, for the initial size distribution of planetesimals to be consistent with the data, their size distribution should steepen at sizes below about one kilometer. In other words, a protoplanetary disc that has successfully built planetesimals with a mass distribution slope of  $\alpha = 1.6$  must also contain a substantial amount of smaller, sub-kilometer-sized solids from the very beginning.

What is the minimum size of those “additional” objects? At any time of the collisional evolution, they should be large enough to not get collisionally depleted by that time. Figure 7 plots collisional lifetimes of different-sized objects in one of the ACE runs discussed above. Yellow curves present the  $M_1/M_2 = 1/20$  (or  $s_t = 1.4$  km) model for monolithic

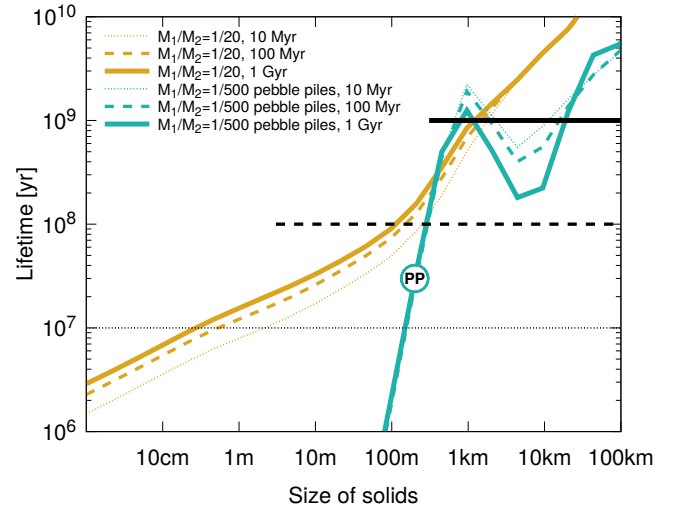


**Figure 7.** Collisional lifetimes of different-sized solids in two ACE runs (yellow and cyan, same colours as in previous figures) after 10 Myr (thin dotted), 100 Myr (medium dashed) and 1 Gyr (think solid) of collisional evolution. These three characteristic ages themselves are shown with horizontal straight lines of the same linestyles.

planetesimals which — as shown above — reproduces the observed emission at all ages from  $\sim 10$  Myr to  $\sim 1$  Gyr reasonably well. It is seen that the objects should be larger than at least a few meters in size to survive the first 10 Myr. At 100 Myr, the minimum radius should be about 100 m. At 1 Gyr, it grows to at least one kilometer. We can conclude that, to sustain the observed amount of emission, the disc must contain solids in the size range from  $\sim 1$  m to  $\sim 1$  km, with a size distribution close to Dohnanyi’s ( $\alpha \approx 1.8\dots 1.9$ ).

In a standard, “slow-growth” scenario, such objects indeed appear as a natural aftermath of formation of large bodies (e.g., [Kenyon & Bromley 2008](#); [Kobayashi et al. 2010](#); [Kobayashi & Löhne 2014](#); [Kobayashi et al. 2016](#)). As explained in Section 2.4, growth of larger bodies in this scenario keeps pace with fragmentation at smaller sizes. At early stages, when a big amount of gas is still present in a protoplanetary disc, the collisional cascade is stalled at around 1–10 meter sizes, because the relative velocities of smaller objects are damped by the ambient gas. However, once gas depletion becomes significant, collisional cascade promptly extends to dust sizes. As a result, by the time of the gas dispersal one expects a Dohnanyi-like slope at sizes below about a kilometer and a shallower slope for larger bodies that have grown in the disc (H. Kobayashi, pers. comm.).

##### 4.2 Discs of “pebble-pile” planetesimals

We now turn to a discussion of the case where planetesimals are assumed to be pebble piles and are described by the alternative  $Q_D^*$ . The cyan curves in Fig. 6 demonstrate that the simulated brightness evolution is not inconsistent with the sample, even if population 1 is nearly absent (we took  $M_1/M_2 = 1/500$ ). In contrast to monolithic objects, pebble piles generate a considerable amount of dust early on. As discussed above, this is because even collisions with much smaller projectiles, which are quite frequent, are sufficient to



disrupt pebble piles. As a result, their collisional lifetimes are very short, dropping to below 1 Myr for planetesimals smaller than 100 meters in radius (see cyan curve in Fig. 7).

Still, the dust brightness curves in Fig. 6 might be too flat, not matching closely a gentle long-term decay that is best visible in the [Chen et al. \(2014\)](#) sample. However, the underlying prescription (2) of  $Q_D^*$  used in the simulation should only be considered as a rough proxy of how the strength of “pebble piles” may look like in reality. If the tensile strength of dust is higher than in our model, or if the minimum of  $Q_D^*$  at meter sizes is deeper than in Eq. (3), then the discs will be brighter at young ages (see a discussion in Section 5.4). Also, assuming smaller pebbles — e.g., 1 mm instead of 1 cm — would help, since shorter collisional lifetimes of tinier pebbles would enhance dust production early on. In fact, pebbles of a millimeter or even smaller sizes can be expected in outer zones of the discs (see, e.g., Fig. 3a in [Johansen et al. 2014](#)). This is because the particle sizes that correspond to the “right” Stokes numbers  $St \sim 0.01\text{--}0.1$  (at which concentration by streaming instability is efficient) decrease at larger distances from the star (e.g. [Carrera et al. 2017](#)). This or that way, it is likely that more realistic models would provide a better match to the observed evolution.

The low fragmentation energy of pebble piles also implies that the disc is devoid of small, sub-km-sized planetesimals (see cyan curve in Fig. 4). This prediction is potentially testable with the Solar System objects. We will discuss this in more detail in Section 5.1.

### 4.3 Total masses of bright debris discs

An inspection of Fig. 6 uncovers a problem that may have been overlooked previously. It concerns the brighter discs, especially in the [Chen et al. \(2014\)](#) sample. Even if we discard the brightest outliers, as discussed in Section 3, the total disc mass required to reproduce bright discs with the models is as large as  $\sim 1000M_\oplus$ . This is true for both monolithic and pebble-pile  $Q_D^*$  prescriptions.

The required total mass of the disc increases with decreasing  $M_1/M_2$  ratio, i.e., if a heavier population 2 is added. However, large total disc masses have already appeared in previous works, based on “traditional” models without population 2. For example, [Wyatt & Dent \(2002\)](#) require at 20–30 $M_\oplus$  in bodies with radius of less than 2 km, which would translate to  $\sim 200\text{--}300M_\oplus$  in 200 km-sized objects, to explain the disc of Fomalhaut. The “high-mass discs” with a dust mass of 0.1  $M_\oplus$  investigated in [Thébault & Augereau \(2007\)](#) imply 190–850 $M_\oplus$  in planetesimals of up to 50 km in radius (see their Table 2). [Müller et al. \(2010\)](#) derive 50–60 $M_\oplus$  in bodies smaller than 74 km for the Vega disc. [Kobayashi & Löhne \(2014\)](#) reproduce the evolution of discs around solar-type stars with 2 AU-wide rings with a radius of 30 AU, containing 45 $M_\oplus$  in 100 km-sized planetesimals. [Schüppler et al. \(2016\)](#) obtain 165 $M_\oplus$  for bodies up to 50 km in size to explain the disc around  $\iota^1$  Eridani.

How massive is an outer planetesimal belt actually allowed to be? Let us consider an initial protoplanetary disc (PPD), which is a progenitor to the debris disc in question. Obviously, it should be lighter than the central star, so let us assume the maximum initial PPD mass is  $0.1M_\star$ . For simplicity, let the central star be sun-like. Assuming a standard gas-to-dust ratio of 100:1, we conclude that the maximum

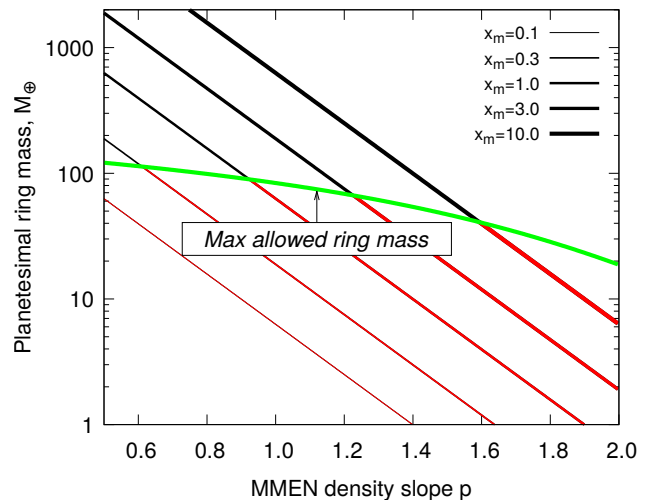


**Figure 8.** The masses of 10 AU-wide planetesimal rings at a distance of 100 AU from the A0-star of  $2.9M_\odot$  in the MMEN model. Solid lines are ring masses as functions of  $p$  (from thin to thick:  $x_m = 0.1, 0.3, 1, 3,$  and  $10$ ). Red portions of these lines correspond to rings such that the total mass of the disc of solids (if the ring cavity were absent) does not exceed 0.001 of the stellar mass. Black portions mean it does; such rings are not allowed. The green line separating red and black represents the maximum allowed ring masses.

total mass in solids in the entire disc is  $0.001M_\odot$ , or  $300M_\oplus$ . By going to more massive stars (e.g. A-stars with 2 or 3 solar masses) or by assuming somewhat lower gas-to-dust ratios (such as the Solar System’s abundances giving 60 : 1, see [Lodders 2003](#)), we can obviously increase that total mass in solids by a factor of two or so, but not much more. This initial constraint is robust. There are simply not more solids available in the PPD than that. This is consistent with the masses of the observed protoplanetary discs. For instance, Fig. 5 in [Williams & Cieza \(2011\)](#) suggests the total masses of PPDs around A-stars to be between 2 and 200 Jupiter masses or 600–60000 $M_\oplus$ , implying 6–600 $M_\oplus$  in solids.

[Kuchner \(2004\)](#) introduced the term “Minimum-Mass Extrasolar Nebula” (MMEN) for extrasolar planetary systems by analogy to the Minimum-Mass Solar Nebula ([Weidenschilling 1977](#); [Hayashi 1981](#)) for our Solar System. The MMEN concept parameterizes the surface density distribution in a PPD by two parameters, the density scaling  $x_m$  and the radial slope  $p$  (such that MMSN has  $x_m = 1$  and  $p = 1.5$ ). Using MMEN, we can easily estimate the solid mass sitting in the outer zone of a certain radius (e.g., 100 AU) and a certain width (e.g., 10 AU). The result (green line in Fig. 8) is 20–130 $M_\oplus$  for discs of A0-stars.

This estimate tacitly assumed that there was no substantial radial transport of solids at earlier phases. However, radial drift in combination with other processes acting at the planetesimal formation phase displaces the solids radially. As a result, the density profile of planetesimals differs from the initial density profile of solids ([Carrera et al. 2017](#)). Another possibility is scattering the planetesimals outward by giant planets later on. This is similar to the “implanted Kuiper belt” scenario of [Levison et al. \(2008\)](#). The mass in giant planets needed for such a displacement is moderate. For instance, to displace 100 $M_\oplus$  outward one would need

about the same mass in giants, so one Saturn or six Neptunes would do. A caveat is that most of the planetesimals will be ejected to interstellar space, and some will fall down to the star. Only a moderate fraction will be implanted to the outer zone we are talking about.

The estimates above are also consistent with predictions of planetesimal formation simulations. Assuming a PPD of  $0.1M_{\star}$  with  $p = 1$ , [Carrera et al. \(2017\)](#) robustly produce a total of 80–150 $M_{\oplus}$  in planetesimals, of which a 60–130 $M_{\oplus}$  are located outside 100 AU.

In summary, several 100 $M_{\oplus}$  is the absolute upper limit on the planetesimal disc mass, whereas collisional models – both previous ones and those considered here – often require much larger masses. We will refer to this as a “disc mass problem” and discuss possible solutions to it in Section 5.

## 5 DISCUSSION

A comparison of models to the debris disc samples has led us to two important findings. One is that debris disc evolution can be successfully reproduced both with the slow-growth and particle concentration scenarios of planetesimal formation. Can we distinguish between the two? Another one is what we call “the disc mass problem.” We have found a discrepancy between the planetesimal disc masses expected from their formation models (likely  $\sim 100M_{\oplus}$ , but not more than a few 100s  $M_{\oplus}$ ) and masses needed to reproduce the observed emission of the brightest debris discs (up to 1000 $M_{\oplus}$  in rings of 10 AU in width). Is it possible to make the total mass of a planetesimal belt smaller, while keeping the same amount of visible dust?

We now try to answer these questions, the first one in Sect. 5.1 and the second one in Sect. 5.2–5.6. As we will see, especially the disc mass problem may require addressing more fundamental aspects of debris discs, whose importance goes beyond that particular problem.

### 5.1 Slow growth or pebble concentration?

Although we cannot discriminate between the two possible routes of planetesimal formation from the analysis of dust fluxes, one possible way to distinguish between them is through the drastically different predictions they make for the amount of sub-km-sized bodies. This is of little help for debris discs around other stars where such objects are not accessible, but at least we may look at our Solar System where sub-km-sized bodies are directly observable. In the present-day Kuiper belt, the spatial density of objects is so low that only the objects smaller than several tens of meters have collisional lifetimes shorter than the age of the Solar System ([Vitense et al. 2012](#)). In contrast to extrasolar debris discs, it is these sub-km-sized bodies in the Kuiper belt that are located at the top of the collisional cascade and serve as the actual source of dust. To be consistent with spacecraft dust detections in the outer Solar System, these bodies should be present in amounts much lower than what would be expected by Dohnanyi-like extrapolation from the observed, 10–100 km-sized transneptunian objects to sub-kilometer sizes. Consistently, [Fulle & Blum \(2017\)](#) point out that the crater density observed on

the bodies in the outer Solar System is low, suggesting that the number of comets smaller than a few kilometers is lower than assumed so far. Closer to the Sun, the size distribution slope of asteroids in comet-like orbits flattens below about one kilometer in size ([Kim et al. 2014](#)). Finally, [Trilling et al. \(2017\)](#) analyzed the size distribution of near-Earth asteroids from 1 km down to 10 meters and found that there are a factor of ten fewer small objects than assumed previously. All this seems to speak for the suggested reduced amount of such bodies in debris discs and thus, to favour the pebble concentration scenario. There is also more direct empirical evidence that comets in the Solar System likely formed through the gentle gravitational collapse of a bound clump of mm-sized pebbles, intermixed with microscopic ice particles. Using the results obtained with a suite of instruments on-board Rosetta mission to comet 67P/Churyumov-Gerasimenko, [Blum et al. \(2017\)](#) found this formation scenario to be compatible with the measured global porosity, homogeneity, tensile strength, thermal inertia, vertical temperature profiles, sizes and porosities of emitted dust, and the water-vapour production rate of the comet. The caveat is that we do not know how representative 67P is for the entire cometary population, and how representative the Solar System is for other planetary systems.

### 5.2 No big planetesimals?

At a first glance, a simple remedy to the disc mass problem would be to assume that the planetesimals larger than a kilometer in size are completely absent. Indeed, it is known that to sustain the observed level of brightness for typical debris discs over Gyrs, kilometer-sized planetesimals would suffice (e.g., [Löhne et al. 2012](#)). This can also be seen in our simulations. Figure 7 suggests that lifetimes of all objects smaller than 1–10 km are typically shorter than systems’ ages, so that their size distribution is set by the collisional cascade. In contrast, the planetesimals larger than 10 km in size essentially retain their primordial distribution. They make a minor contribution to the cascade, only producing a moderate amount of dust through cratering collisions.

Since the disc mass is proportional to  $s_{\max}^{6-3\alpha}$ , replacing  $s_{\max} = 100$  km with  $s_{\max} = 1$  km would reduce the belt mass by a factor of 5 for  $\alpha = 1.88$  or even by a factor of 250 for  $\alpha = 1.6$ . However, that would challenge the planetesimal formation models that robustly predict largest planetesimals to be 100s of km in size ([Schäfer et al. 2017](#)). Furthermore, without large planetesimals it would be difficult to explain why the discs produce dust at all. Dust is only produced if the planetesimals have sufficiently high relative velocities, i.e., non-zero eccentricities and/or inclinations. Stirring may come from embedded big planetesimals or from planets in the inner cavities of the discs. In the former case, this directly requires large planetesimals to be present. In the latter case, it would be difficult to understand why planetary-sized bodies have formed successfully closer in, whereas 100km-sized planetesimals slightly farther out have not.

Even though the predicted slope of the size distribution of planetesimals probably extends to large sizes, it remains possible that the actual  $s_{\max}$  is by a factor of several smaller than assumed here. For instance, recent simulations by [Klahr & Schreiber \(2016\)](#) produce planetesimals with sizes peaking at  $\approx 50$  km. Such sizes would imply the re-

quired total masses of debris discs by a factor of 2–4 smaller, reducing the tension between the debris disc models and the data.

### 5.3 More recent origin of debris?

All the results obtained above rely on two basic assumptions. One is an assumption that the observed debris dust is produced in a collisional cascade, which is treated statistically. This means that even the largest colliding bodies are considered to be numerous enough to be part of a continuous size distribution (Tanaka & Nakazawa 1994). Another assumption is that the “collisional age” of the systems, i.e., the time elapsed since the ignition of the cascade, is equal to the system’s age. In principle, we can question both. Especially for the brightest discs at older ages, it is possible that a recent giant impact caused a temporary brightness increase (e.g. Kenyon & Bromley 2005; Jackson et al. 2014; Kral et al. 2015; Genda et al. 2015). Also, “delayed stirring” (Dominik & Decin 2003; Wyatt 2008) is possible, implying that the cascade was triggered later in the system’s history — for instance following the formation of Pluto-sized planetesimals in the disc (Kenyon & Bromley 2008), when the stirring front from planets in the inner cavities has reached the disc (Mustill & Wyatt 2009), or by late dynamical instabilities caused by planetary migration or scattering (Booth et al. 2009). In all these cases, the total mass of a debris disc of a given brightness would be lower than derived in this work.

### 5.4 Overall steeper size distribution?

Another way to get more dust from a given total mass would be to assume that the overall slope of the size distribution of solids from dust to km-sized planetesimals is steeper than collisional simulations suggest. However, that slope cannot simply be varied, as it is set by the cascade. Specifically, it depends on the slope of  $Q_D^*(s)$  (O’Brien & Greenberg 2003). This can easily be explained with simple qualitative arguments. The amount of dust is determined by the product of the dust production rate and lifetime. The production rate equals mass loss rate of planetesimals (since the cascade relays the mass from planetesimals to dust), while the dust lifetime is set by  $Q_D^*$  (being proportional to  $(Q_D^*)^{5/6}$ , see Wyatt et al. 2007a). In turn, the mass loss rate of planetesimals is set by their  $Q_D^*$ . So, effectively, the mass ratio between dust and planetesimals depends on the respective  $Q_D^*$  ratio. Making the planetesimals at the top end of the cascade weaker (which corresponds to steepening the  $Q_D^*$  slope) should have a similar effect as directly strengthening the dust. However, the  $Q_D^*$  of the biggest planetesimals is largely determined by gravity and thus is quite certain. Thus the only way to increase the amount of visible dust is to assume that the dust is “harder”, i.e., has a larger  $Q_D^*$ .

The above reasoning also means that the  $Q_D^*$  of intermediate, centimeter- to kilometer-sized bodies should be unimportant for the long-term evolution of discs. This is readily confirmed by our simulations. To see this, it is sufficient to compare the cyan curve in Fig. 4 to the other curves. The cyan curve employed an alternative critical fragmentation energy model to describe the destruction of pebble-pile, “macrogranular” planetesimals, while the others used a stan-

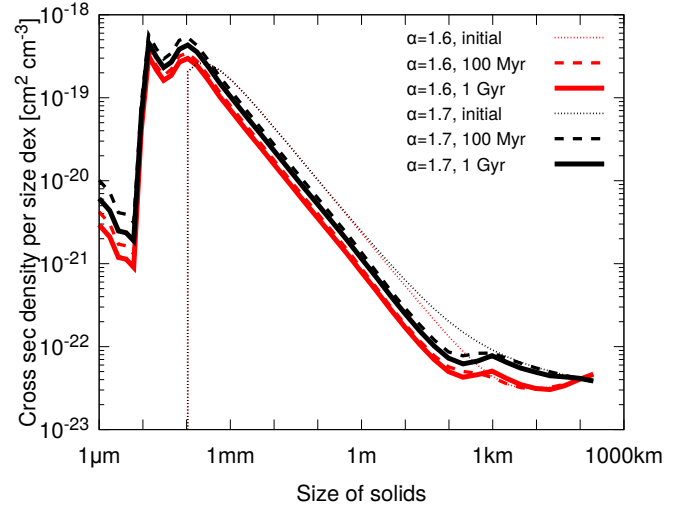


**Figure 9.** Size distributions of solids in the  $M_1 + M_2 = 100M_\oplus$  and  $M_1/M_2 = 1/20$  model with a standard  $Q_D^*$  prescription in two cases: the reference one with  $\alpha = 1.6$  (red) and the one assuming  $\alpha = 1.7$  instead (black). Lines from thin dotted to thick solid show the distributions at 0 Myr, 100 Myr, and 1 Gyr.

dard prescription. Remember that the alternative model predicts much weaker planetesimals with radii between the pebble size and the sizes where the strength starts to be dominated by gravity, but does not change much the strength of both the *dust* and *large planetesimals*. A comparison shows that all these simulations predict a comparable amount of dust after 100 Myr of evolution. Note that this is only true after the disc has evolved long enough for the big bodies in the gravity regime to get involved in the cascade (which is certainly the case after 100 Myr). As discussed above, early on the debris discs composed of pebble piles are brighter than the discs of “monolithic” planetesimals.

### 5.5 A steeper size distribution of large planetesimals?

The planetesimal formation models derive the slope  $\alpha = 1.6$  with some uncertainty. We checked whether a somewhat steeper slope of the population 2, namely  $\alpha = 1.7$ , would change the amount of visible dust markedly. This turned out not to be the case (Fig. 9). After 100 Myr of collisional evolution, the cross section – and emission flux – of the dust increases by less than a factor of two. At 1 Gyr, it is even smaller.

### 5.6 Non-collisional dust production?

In principle, one can question a standard view that visible dust in Kuiper-belt analogs is produced solely via collisions. As an example, Jacobson et al. (2014) argue that for main-belt asteroids smaller than a few kilometers in size, YORP-induced rotational disruption significantly contributes to the erosion even exceeding the effects of collisional fragmentation. Several erosion-like mechanisms may also enhance dust production. We know that planetesimals in debris discs contain ices. For instance, the presence of  $\sim 10\%$  of CO ice has been deduced from CO gas detections (e.g., Kral et al.

2017). The sublimation temperature of the most volatile ices such as CO, CH<sub>4</sub>, and N<sub>2</sub> are lower than  $\sim 45$  K (Dodson-Robinson et al. 2009), allowing them to sublimate at Kuiper-belt distances from the primary stars. Another possibility would be photodesorption of ices, which should be most efficient around A-type stars considered here (e.g., Grigorieva et al. 2007). Such mechanisms of ice erosion might cause a direct, non-collisional release of dust particles from an icy-rocky matrix at the surfaces of planetesimals in a “cometary” way.

## 6 CONCLUSIONS

Our key results are as follows:

(i) The long-term evolution of debris discs is largely determined by the collisional strength of solids at both ends of the size distribution, i.e., large planetesimals in the gravity regime and dust. However, this is different at early stages of debris disc evolution, when the system is younger than the collisional lifetime of planetesimals kept together by gravity. The temporal evolution of debris discs at younger ages is sensitive to the assumed fragmentation laws of intermediate-sized planetesimals, and thus to their internal structure. Discs of “monolithic” planetesimals and those of “pebble piles” exhibit different evolutionary curves. This shows a principal possibility to constrain structure and porosity of planetesimals from the observations of young debris discs. However, it is not easy, since the dust fluxes also depend on other parameters such as the birth size distribution of planetesimals, see conclusions (ii) and (iii) below.

(ii) Assuming “monolithic” planetesimals, as implied by the standard planetesimal formation scenario, we are able to reproduce the observed debris disc brightness evolution. The requirement is that planetesimal belts left after the time of the gas dispersal must include a substantial population of sub-kilometer-sized planetesimals. For example, a population of objects with sizes from about 1 meter to about 1 kilometer and a Dohnanyi-like slope  $\alpha \approx 1.8\dots 1.9$  would suffice. This population is expected in the standard planetesimal formation scenario as well, since the growth of larger bodies in a protoplanetary disc in that scenario proceeds concurrently with fragmentation at smaller sizes that establishes such a slope by the time of gas dispersal.

(iii) For planetesimals with a pebble-pile structure, as expected in the particle concentration models, this additional population of small planetesimals may not be required — and is not predicted. Taking the initial size distribution with a slope  $\alpha \approx 1.6$  between a few kilometers and a few hundred kilometers and assuming planetesimals to be pebble piles, as suggested by these models, we are also able to roughly reproduce the average luminosities of debris discs at all ages.

(iv) While our modelling shows that the observed brightness evolution of debris discs is compatible with both monolithic and pebble-pile planetesimals, there is a possibility to discriminate between the two cases for the Solar System. Both the relative paucity of sub-km-sized small bodies and close-up studies of comet 67/P with Rosetta mission seem to favour the fragile, pebble-pile composition of planetesimals in our own debris disc, supporting the “particle concentration” scenario of their formation.

(v) Explaining debris discs in the samples with a brightness above the average uncovers a “disc mass problem.” For such discs to be reproduced by collisional simulations, the total disc mass located within a 10 AU ring should be on the order of  $\sim 1000M_{\oplus}$ . This is more than the total mass of solids available in the protoplanetary progenitors of debris discs, which should not exceed a few 100s  $M_{\oplus}$ . The problem appears for all initial size spectra of planetesimals and their collisional strengths that we invoked in this study.

(vi) We consider several possibilities, one or more of which may help to resolve the disc mass problem. Some systems may have experienced recent major break-up of big planetesimals. In some other systems, the collisional cascade may not have ignited immediately after the gas dispersal (“delayed stirring”). In still other systems, ages are quite uncertain; younger ages would imply less total mass. It is also possible that sublimation or photodesorption of ices enhances purely collisional dust production from parent planetesimals by releasing dust from their surfaces; this would reduce the total mass needed to sustain the observed amount of dust as well.

## ACKNOWLEDGEMENTS

We are grateful to Mark Booth for commenting on the manuscript and Hiroshi Kobayashi for providing us with the details of his planetesimal growth simulations. A speedy and insightful referee report by an anonymous reviewer is very much appreciated. AVK, TL, and JB thank the *Deutsche Forschungsgemeinschaft* (DFG) for financial support through grants Kr 2164/13-1, Lo 1715/2-1, and Bl 298/24-1, respectively. AJ thanks the Knut and Alice Wallenberg Foundation (grants 2012.0150, 2014.0017, 2014.0048), the Swedish Research Council (grant 2014-5775) and the European Research Council (ERC Consolidator Grant 724687-PLANETESYS) for their financial support.

## REFERENCES

- Benz W., Asphaug E., 1999, *Icarus*, **142**, 5  
 Blum J., et al., 2017, preprint, ([arXiv:1710.07846](https://arxiv.org/abs/1710.07846))  
 Booth M., Wyatt M. C., Morbidelli A., Moro-Martín A., Levison H. F., 2009, *MNRAS*, **399**, 385  
 Bukhari Syed M., Blum J., Wahlberg Jansson K., Johansen A., 2017, *Astrophys. J.*, **834**, 145  
 Burns J. A., Lamy P. L., Soter S., 1979, *Icarus*, **40**, 1  
 Campo Bagatin A., Cellino A., Davis D. R., Farinella P., Paolicchi P., 1994, *Planet. Space Sci.*, **42**, 1079  
 Carrera D., Gorti U., Johansen A., Davies M. B., 2017, *Astrophys. J.*, **839**, 16  
 Chen C. H., Mittal T., Kuchner M., Forrest W. J., Lisse C. M., Manoj P., Sargent B. A., Watson D. M., 2014, *Astrophys. J. Suppl.*, **211**, 25  
 Cuzzi J. N., Hogan R. C., Shariff K., 2008, *Astrophys. J.*, **687**, 1432  
 Cuzzi J. N., Hogan R. C., Bottke W. F., 2010, *Icarus*, **208**, 518  
 Dodson-Robinson S. E., Willacy K., Bodenheimer P., Turner N. J., Beichman C. A., 2009, *Icarus*, **200**, 672  
 Dohnanyi J. S., 1969, *J. Geophys. Res.*, **74**, 2531  
 Dominik C., Decin G., 2003, *Astrophys. J.*, **598**, 626  
 Donaldson J. K., Lebreton J., Roberge A., Augereau J.-C., Krivov A. V., 2013, *ApJ*, **772**, 17



- Fulle M., Blum J., 2017, *MNRAS*, 469, S39
- Fulle M., et al., 2016, *MNRAS*, 462, S132
- Gáspár A., Psaltis D., Rieke G. H., Özel F., 2012, *Astrophys. J.*, 754, 74
- Gáspár A., Rieke G. H., Balog Z., 2013, *Astrophys. J.*, 768, 25
- Geiler F., Krivov A. V., 2017, *MNRAS*, 468, 959
- Genda H., Kobayashi H., Kokubo E., 2015, *Astrophys. J.*, 810, 136
- Grigorieva A., Thébault P., Artymowicz P., Brandeker A., 2007, *Astron. Astrophys.*, 475, 755
- Haghighipour N., Boss A. P., 2003, *Astrophys. J.*, 598, 1301
- Hayashi C., 1981, *Prog. Theor. Phys. Suppl.*, 70, 35
- Jackson A. P., Wyatt M. C., Bonsor A., Veras D., 2014, *MNRAS*, 440, 3757
- Jacobson S. A., Marzari F., Rossi A., Scheeres D. J., Davis D. R., 2014, *MNRAS*, 439, L95
- Johansen A., Oishi J. S., Low M.-M. M., Klahr H., Henning T., Youdin A., 2007, *Nature*, 448, 1022
- Johansen A., Youdin A., Klahr H., 2009, *Astrophys. J.*, 697, 1269
- Johansen A., Blum J., Tanaka H., Ormel C., Bizzarro M., Rickman H., 2014, in Beuther H., Klessen R., Dullemond C., Henning T., eds, *Protostars and Planets VI*. U. Arizona Press, Tucson, pp 547–570
- Johansen A., Mac Low M.-M., Lacerda P., Bizzarro M., 2015, *Science Advances*, 1, 1500109
- Kennedy G. M., Wyatt M. C., 2010, *MNRAS*, 405, 1253
- Kenyon S. J., Bromley B. C., 2005, *Astron. J.*, 130, 269
- Kenyon S. J., Bromley B. C., 2008, *Astrophys. J. Suppl.*, 179, 451
- Kenyon S. J., Luu J. X., 1999, *Astrophys. J.*, 526, 465
- Kim Y., Ishiguro M., Usui F., 2014, *Astrophys. J.*, 789, 151
- Klahr H., Schreiber A., 2016, in Chesley S. R., Morbidelli A., Jedicke R., Farnocchia D., eds, *IAU Symposium Vol. 318, Asteroids: New Observations, New Models*. pp 1–8, doi:10.1017/S1743921315010406
- Kobayashi H., Löhne T., 2014, *MNRAS*, 442, 3266
- Kobayashi H., Tanaka H., Krivov A. V., Inaba S., 2010, *Icarus*, 209, 836
- Kobayashi H., Tanaka H., Okuzumi S., 2016, *Astrophys. J.*, 817, 105
- Kral Q., Thébault P., Augereau J.-C., Boccaletti A., Charnoz S., 2015, *A&A*, 573, A39
- Kral Q., Matrà L., Wyatt M. C., Kennedy G. M., 2017, *MNRAS*, 469, 521
- Krivov A. V., 2010, *Research in Astron. Astrophys.*, 10, 383
- Krivov A. V., Löhne T., Sremčević M., 2006, *A&A*, 455, 509
- Krivov A. V., Müller S., Löhne T., Mutschke H., 2008, *Astrophys. J.*, 687, 608
- Krivov A. V., et al., 2013, *Astrophys. J.*, 772, 32
- Kuchner M. J., 2004, *Astrophys. J.*, 612, 1147
- Lebreton J., et al., 2012, *Astron. Astrophys.*, 539, A17
- Leinhardt Z. M., Stewart S. T., 2012, *Astrophys. J.*, 745, 79
- Levison H. F., Morbidelli A., Vanlaerhoven C., Gomes R., Tsiganis K., 2008, *Icarus*, 196, 258
- Lodders K., 2003, *Astrophys. J.*, 591, 1220
- Löhne T., Krivov A. V., Rodmann J., 2008, *ApJ*, 673, 1123
- Löhne T., et al., 2012, *A&A*, 537, A110
- Löhne T., Krivov A. V., Kirchschrager F., Sende J. A., Wolf S., 2017, *Astron. Astrophys.*, 605, A7
- Matthews B. C., Krivov A. V., Wyatt M. C., Bryden G., Eiroa C., 2014, in Beuther H., Klessen R., Dullemond C., Henning T., eds, *Protostars and Planets VI*. U. Arizona Press, Tucson, pp 521–544
- Moór A., Abraham P., Deras A., Kiss C., Kiss L. L., Apai D., Grady C., Henning T., 2006, *Astrophys. J.*, 644, 525
- Moór A., et al., 2011, *Astrophys. J. Lett.*, 740, L7
- Morbidelli A., Levison H. F., Bottke W. F., Dones L., Nesvorný D., 2009, *Icarus*, 202, 310
- Müller S., Löhne T., Krivov A. V., 2010, *ApJ*, 708, 1728
- Mustill A. J., Wyatt M. C., 2009, *MNRAS*, 399, 1403
- O’Brien D. P., Greenberg R., 2003, *Icarus*, 164, 334
- Okuzumi S., Tanaka H., Kobayashi H., Wada K., 2012, *Astrophys. J.*, 752, 106
- Pawellek N., Krivov A. V., 2015, *MNRAS*, 454, 3207
- Pawellek N., Krivov A. V., Marshall J. P., Montesinos B., Abraham P., Moór A., Bryden G., Eiroa C., 2014, *Astrophys. J.*, 792, 65
- Reidemeister M., Krivov A. V., Stark C. C., Augereau J.-C., Löhne T., Müller S., 2011, *Astron. Astrophys.*, 527, A57
- Rhee J. H., Song I., Zuckerman B., McElwain M., 2007, *Astrophys. J.*, 660, 1556
- Rieke G. H., et al., 2005, *Astrophys. J.*, 620, 1010
- Schäfer U., Yang C.-C., Johansen A., 2017, *Astron. Astrophys.*, 597, A69
- Schüppler C., Löhne T., Krivov A. V., Ertel S., Marshall J. P., Eiroa C., 2014, *Astron. Astrophys.*, 567, A127
- Schüppler C., et al., 2015, *Astron. Astrophys.*, 581, A97
- Schüppler C., Krivov A. V., Löhne T., Booth M., Kirchschrager F., Wolf S., 2016, *MNRAS*, 461, 2146
- Simon J. B., Armitage P. J., Li R., Youdin A. N., 2016, *Astrophys. J.*, 822, 55
- Simon J. B., Armitage P. J., Youdin A. N., Li R., 2017, arXiv:1705.03889,
- Southworth J., Maxted P. F. L., Smalley B., 2005, *Astron. Astrophys.*, 429, 645
- Stewart S. T., Leinhardt Z. M., 2009, *Astrophys. J. Lett.*, 691, L133
- Su K. Y. L., et al., 2006, *ApJ*, 653, 675
- Tanaka H., Nakazawa K., 1994, *Icarus*, 107, 404
- Thébault P., Augereau J.-C., 2007, *Astron. Astrophys.*, 472, 169
- Thébault P., Augereau J.-C., Beust H., 2003, *Astron. Astrophys.*, 408, 775
- Thureau N. D., et al., 2014, *MNRAS*, 445, 2558
- Trilling D. E., Valdes F., Allen L., James D., Fuentes C., Herrera D., Axelrod T., Rajagopal J., 2017, arXiv:1707.04066,
- Vitense C., Krivov A. V., Kobayashi H., Löhne T., 2012, *Astron. Astrophys.*, 540, A30
- Wada K., Tanaka H., Suyama T., Kimura H., Yamamoto T., 2009, *Astrophys. J.*, 702, 1490
- Wada K., Tanaka H., Okuzumi S., Kobayashi H., Suyama T., Kimura H., Yamamoto T., 2013, *Astron. Astrophys.*, 559, A62
- Weidenschilling S. J., 1977, *Astrophys. Space Sci.*, 51, 153
- Whizin A. D., Blum J., Colwell J. E., 2017, *Astrophys. J.*, 836, 94
- Williams J. P., Cieza L. A., 2011, *Ann. Rev. Astron. Astrophys.*, 49, 67
- Windmark F., Birnstiel T., Güttler C., Blum J., Dullemond C. P., Henning T., 2012, *Astron. Astrophys.*, 540, A73
- Wurm G., Paraskov G., Krauss O., 2005, *Icarus*, 178, 253
- Wyatt M. C., 2008, *Ann. Rev. Astron. Astrophys.*, 46, 339
- Wyatt M. C., Dent W. R. F., 2002, *MNRAS*, 334, 589
- Wyatt M. C., Dermott S. F., Telesco C. M., Fisher R. S., Grogan K., Holmes E. K., Piña R. K., 1999, *Astrophys. J.*, 527, 918
- Wyatt M. C., Smith R., Greaves J. S., Beichman C. A., Bryden G., Lisse C. M., 2007a, *Astrophys. J.*, 658, 569
- Wyatt M. C., Smith R., Su K. Y. L., Rieke G. H., Greaves J. S., Beichman C. A., Bryden G., 2007b, *ApJ*, 663, 365
- Wyatt M. C., Clarke C. J., Booth M., 2011, *Celest. Mech. Dynam. Astron.*, 111, 1

This paper has been typeset from a  $\text{\TeX}/\text{\LaTeX}$  file prepared by the author.